MAGNETIC FIELDS IN STAR-FORMING MOLECULAR CLOUDS. I. THE FIRST POLARIMETRY OF OMC-3 IN ORION A

BRENDA C. MATTHEWS[1] AND CHRISTINE D. WILSON[1]

ABSTRACT

The first polarimetric images of the OMC-3 region of the Orion A filamentary molecular cloud are presented. Using the new imaging polarimeter on the Submillimeter Common User Bolometric Array at the James Clerk Maxwell Telescope, we have detected polarized thermal emission at 850 μm from dust along a 6' length of the dense filament. The polarization pattern is highly ordered and is aligned with the long axis of the filament throughout most of the region, diverging only near the southern boundary by 30°–50°. If the polarization arises from thermal emission of dust grains aligned via either paramagnetic inclusions or radiative torques, this configuration indicates a plane-of-sky magnetic field which is normal to the filament along most of its length. The mean percentage polarization is 4.2% with a 1 σ dispersion of 1%. This region is part of the integral-shaped filament, and active star formation is ongoing along its length, with only two of nine dust condensations in our field lacking evidence of outflow activity. The outflow directions do not appear to be consistently correlated with the direction of the plane-of-sky field or the filament structure itself. Depolarization toward the filament center, previously detected in many other star-forming cores and protostars, is also evident in our data.

Subject headings: ISM: clouds — ISM: magnetic fields — ISM: molecules — polarization — stars: formation — submillimeter

1. INTRODUCTION

It is now well established that magnetic fields play a significant role in the evolution of molecular clouds and their associated star formation (see Heiles et al. 1993 and references therein). At a distance of 500 pc, the Orion complex is the closest star-forming region that is undergoing massive star formation and, as such, has been the object of intense study. Many studies have focused on the region known as OMC-1, a massive cloud core that lies behind the Orion Nebula (M42). This core is embedded in the integral-shaped filament, identified in the ^{13}CO $J = 1–0$ transition by Bally et al. (1987) and most recently mapped at 850 and 450 μm by Johnstone & Bally (1999). The OMC-3 region lies at the northern tip of the filament (Bally et al. 1987) near the H II region NGC 1977 (see Kutner, Evans, & Tucker 1976). Molecular studies reveal the dust temperatures to be considerably cooler ($T \sim 20–25$ K) in the OMC-3 region than in OMC-1 (Chini et al. 1997).

Dust condensations in OMC-3 were identified in 1.3 mm continuum by Chini et al. (1997). An evolutionary sequence has been suggested, with source ages declining as one moves north along the filament. Reipurth, Rodríguez, & Chini (1999) have done a Very Large Array (VLA) search at 6 cm for compact sources in the region and report no sources coincident with the positions of MMS 1 and MMS 4, two of the most northern condensations identified by Chini et al. (1997). Additionally, there is no outflow associated with either source (Yu, Bally, & Devine 1999; Chini et al. 1997; Castets & Langer 1995). These results suggest that these objects may in fact be in a precollapse phase, since outflows are known to be associated with the earliest phases of collapse (Shu, Adams, & Lizano 1987).

Goodman et al. (1995) illustrated that measurements of polarization of background starlight in the optical and near-infrared are not effective tracers of magnetic field structure in dense molecular gas due to poor alignment and/or amorphous dust grain structure. At submillimeter and millimeter wavelengths, aligned, rotating grains produce polarized thermal emission. Draine & Weingartner (1996, 1997) have shown that radiative torques are highly effective at aligning grains of specific sizes (~ 0.2 μm). Lazarian, Goodman, & Myers (1997) suggest that the effects of radiative torques could be comparable to paramagnetic inclusions (Purcell 1975, 1979; Spitzer & McGlynn 1979) at aligning grains in the star-forming interstellar medium. Both these mechanisms result in grains aligned with their long axes perpendicular to the magnetic field.

In this paper, we present 850 μm imaging polarimetry of OMC-3. These data represent the first polarimetry of this active star-forming region and are also some of the first obtained with the new imaging polarimeter at the James Clerk Maxwell Telescope (JCMT). This is the first publication from a project designed to study magnetic-field structure in a variety of molecular clouds in different phases of star formation. In § 2 we describe the polarimeter and the observing and reduction techniques; in § 3 a mosaic of OMC-3 is presented and discussed; § 4 summarizes the results thus far.

2. OBSERVATIONS AND DATA REDUCTION

The observations were taken from 1998 September 5 to 7 using the new imaging polarimeter on Submillimeter Common User Bolometric Array (SCUBA) at the JCMT. These nights were stable, with τ(225 GHz) ranging from 0.05 to 0.07 during the period of observations. Calibration of the polarizer was performed on 1998 September 5 using the Crab Nebula, for which percentage polarization $p = 19.3\% \pm 4\%$ and position angle $\theta = 155° \pm 5°$ were measured.

The polarimeter consists of a rotating quartz half-wave plate and a fixed analyzer that are used to measure linear polarization of thermal emission. The wave plate introduces a phase-lag of one-half wavelength between the plane of polarization along the "fast axis" and the orthogonal

[1] Department of Physics and Astronomy, McMaster University, Hamilton, ON L8S 4M1, Canada.

plane. Rotation of the plate changes the angle between the fast axis and the plane of the incoming source polarization, so a varying component of the polarized emission is retarded. The analyzer is a photolithographically etched grid of 6 μm spacing that transmits only one plane of polarization (by absorbing photons with an E-component parallel to the wires) to SCUBA. The detector thus sees a modulated signal as the wave plate rotates. The variations are used to deduce the percentage polarization and polarization position angle of the source.

Seven pointing centers were observed along the OMC-3 filament, four the first night and only three (slightly shifted in position) on subsequent nights, to provide better coverage of low signal-to-noise regions. Data for each pointing center were co-added to create seven maps of I, $Q = q/I$, and $U = u/I$, where I, q, and u are Stokes parameters. Each polarization cycle consists of 16 integrations at $22.°5$ rotation intervals (i.e., four independent measurements at each angle) in 8 minutes integration time. The brightest source, MMS 6, was observed for only six cycles, or 48 minutes integration time. Observations centered on MMS 1 and MMS 4 required ~ 3 hours integration time. The sensitivity of the SCUBA detector yielded polarization measurements on sources of 0.5 Jy beam^{-1} at the 6 σ level for 4% polarized flux.

For each polarization cycle map, the standard preliminary reduction was done. This included subtraction of sky levels as well as instrumental polarization (IP) for each bolometer. Polarizations less than 1% are unreliable, since the IP has been found to vary by $\pm 0.5\%$ for about 30% of the bolometers. The average IP for all off-axis bolometers is $0.88\% \pm 0.06\%$ at $166° \pm 2°$, while the IP of the central bolometer is $1.08\% \pm 0.10\%$ at $158° \pm 3°$. After correction for source rotation across the array, the Stokes parameters were calculated by comparing measurements offset by $45°$ in wave plate rotation ($90°$ on the sky). The I, Q, and U maps for each pointing center were averaged, and standard deviations were derived by comparing the individual data sets. The maps were then binned spatially by a factor of 2 to yield $6''$ (approximately half-beamwidth) sampling.

At this point, it was necessary to diverge from the standard reduction technique to make mosaics of the I, Q, and U maps before calculating the percentage polarization p and position angle θ. Mosaicing was done using the MAKEMOS tool in Starlink's CCDPACK (a UK-based software package). Variances were used to weight the overlapping data values, and variances were also generated for the map. The calculation of p (and its uncertainty) is given by

$$p = \sqrt{Q^2 + U^2}; \quad dp = p^{-1}\sqrt{(dQ^2Q^2 + dU^2U^2)}. \quad (1)$$

A bias exists that tends to increase the p-value, even when Q and U are consistent with $p = 0$ because p is forced to be positive. The polarization percentages were debiased according to the expression

$$p_{\rm db} = \sqrt{p^2 - dp^2}. \quad (2)$$

The position angle can then be calculated by the following relations:

$$\theta = 0.5 \arctan (U/Q); \quad d\theta = 28.°6/\sigma_p, \quad (3)$$

where σ_p is the ratio $p_{\rm db}/dp$.

The $p_{\rm db}$ values were then thresholded such that $p_{\rm db} \leq 100\%$ and $\sigma_p \geq 2.5$. The position angles can, of course, take

on any value, but we note that offsets of $180°$ cannot be distinguished in linear polarization.

3. RESULTS

3.1. *The Polarization Pattern*

Figure 1 shows the OMC-3 filament in 850 μm continuum (color scale) overlaid with polarization vectors. Only vectors up to 20% are plotted on the figure; 27 vectors in total were omitted. The blue contours indicate where $\sigma_p = 6$ and $\sigma_p = 10$. By equation (3), the vectors enclosed by these contours have $d\theta \leq 5°$ and $d\theta \leq 3°$, respectively. No vectors have $\sigma_p < 2.5$, so no plotted vector has $d\theta > 12°$.

The polarization vectors are well ordered along the filament with the best alignment in the northern region between the sources MMS 1 and MMS 6 (as identified by Chini et al. 1997; see Fig. 1). Since the vectors show a high degree of ordering, it is tempting to think that they are uniform across the field. However, extraction of data subsets centered on each of the four "regions" indicated in Figure 1 illustrates that this is not the case. The distribution of θ in each region is fit by either 1 or 2 Gaussians by minimizing χ^2. The position angle (mean and dispersion) of each of these Gaussians is noted on the figure, as well as the reduced χ^2 of each fit.

The dispersions in θ are relatively narrow when compared with the sample presented in Myers & Goodman (1991) for 26 dark cloud regions. If a single Gaussian is fit to every subregions' distribution (regardless of the goodness of fit), it is found that regions A through D have dispersions of $8°$, $8°$, $9°$, and $12°$, respectively. Such low dispersions were identified only for dark clouds without clusters, i.e., less than 15 associated stars in 1 pc^2 (Myers & Goodman 1991), yet OMC-3 has condensation density of 135 pc^{-2} (taking nine sources in a $6' \times 30''$ area). According to the Myers & Goodman model of uniform and nonuniform field components, this result implies either a low ratio of nonuniform to plane-of-sky uniform components of the magnetic field, or a low number of magnetic field correlation lengths along the line of sight. To implement their analysis fully will require measurement of the line-of-sight component of the magnetic field toward several positions in OMC-3.

It is interesting to compare the changes in the position angle of the filament on the sky with the change in orientation of the polarization vectors. The filament's orientation can be traced easily due to the positions of the condensations themselves which, without exception, are embedded within it. Measuring an angle E of N, three main segments of OMC-3 can be distinguished. From MMS 1 to MMS 6, the filament is at an angle of $\sim 130°$ ($-50°$); this area is covered by regions A and B as denoted on Figure 1. These histograms reveal that the peaks fit to these distributions agree with the position angle of the filament to within $10°$. The situation is similar for region C, which contains MMS 7, the only *IRAS* source in OMC-3 ($05329-0505$). The angle of the filament steepens from MMS 6 to MMS 7 to $\sim 160°$ ($-20°$). The distribution of θ exhibits two peaks in position angle. The strongest peak is in fact at $-19° \pm 7°$, which indicates excellent alignment with the filament. (The uncertainty represents the 1 σ dispersion in the distribution.) However, a second peak exists at $-36° \pm 5°$. Finally, from MMS 7 through MMS 9, the filament aligns north-south (position angle $0°$). None of the polarization vectors exhibit such an angle; instead, the distribution is double
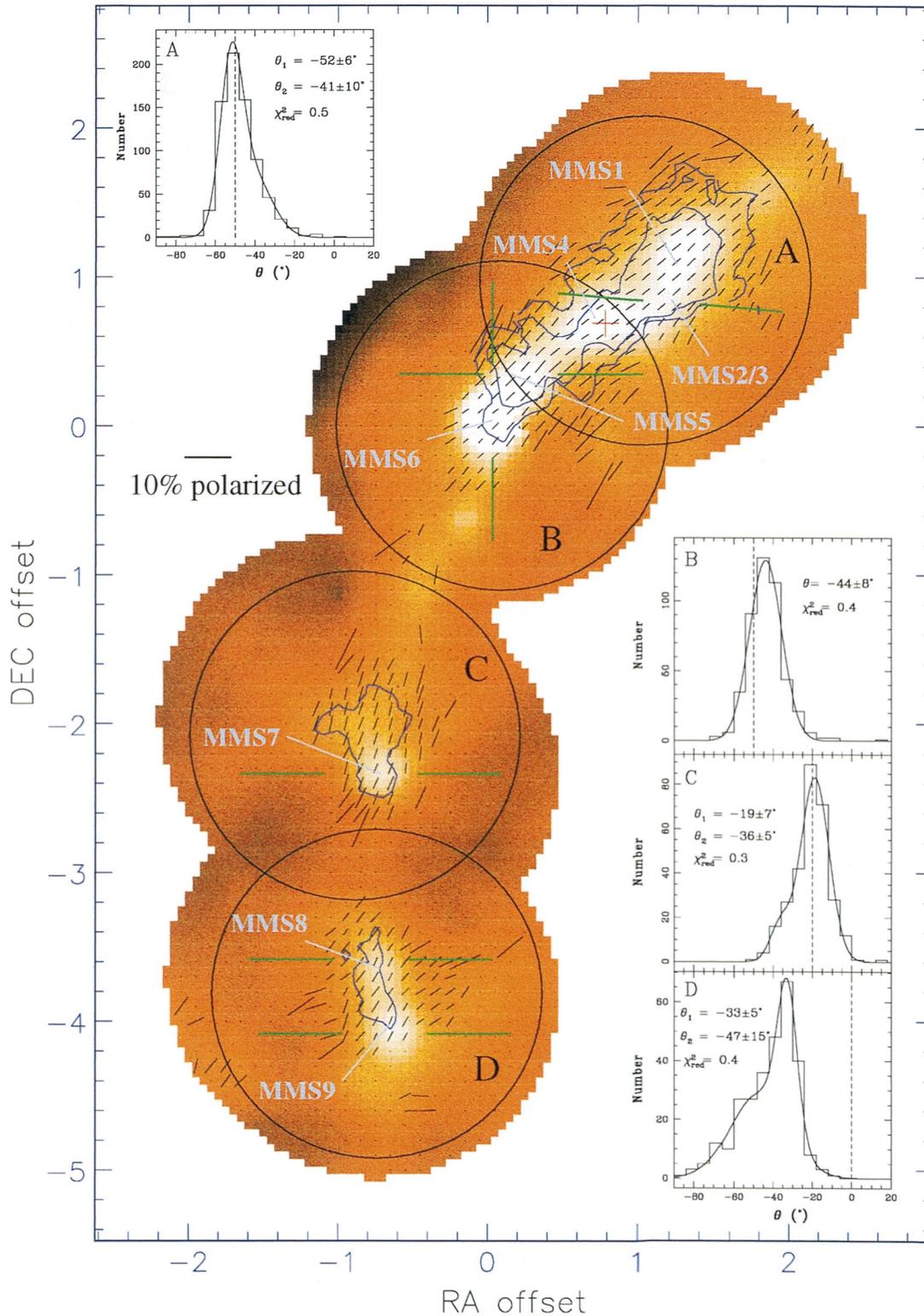
FIG. 1.—The 850 μm polarized emission along OMC-3. The coordinates are arcminute offsets from the position of MMS 6, $\alpha_{1950} = 5^h32^m55^s.6$ and $\delta_{1950} = -5°03'25''$. Color scale indicates variations in uncalibrated I, with a range of -2 to 3σ. Polarization vectors (to a maximum of 20%) are overlain. All vectors shown have $\sigma_p > 2.5$. Blue contours indicate bounds of $\sigma_p = 6$ and $\sigma_p = 10$, respectively. These bounds also indicate where $d\theta < 5°$ and $d\theta < 3°$, respectively. The condensations of Chini et al. (1997) are labeled MMS 1 through MMS 9, and outflow orientations are shown in green. The red cross shows the center of the cut shown in Figure 2. Subregions, labeled A through D, are identified, and the distributions of position angle for each are shown in the histograms. Position angles are grouped to 6° bin widths. To test the form of the distributions, binning was also done with widths of 3° and 12°. The only cases in which the distributions were not consistent were regions A and D with a 12° bin width. In these cases, the double Gaussian profile did not produce a fit to the data. Nevertheless, all single Gaussian fits for these two regions produced reduced χ^2-values greater than 1; hence, single Gaussians are poor fits to these distributions. The parameters of the fits are noted on each figure, as well as the reduced χ^2-values. The dashed lines represent the mean position angle of the *filament* in each region.
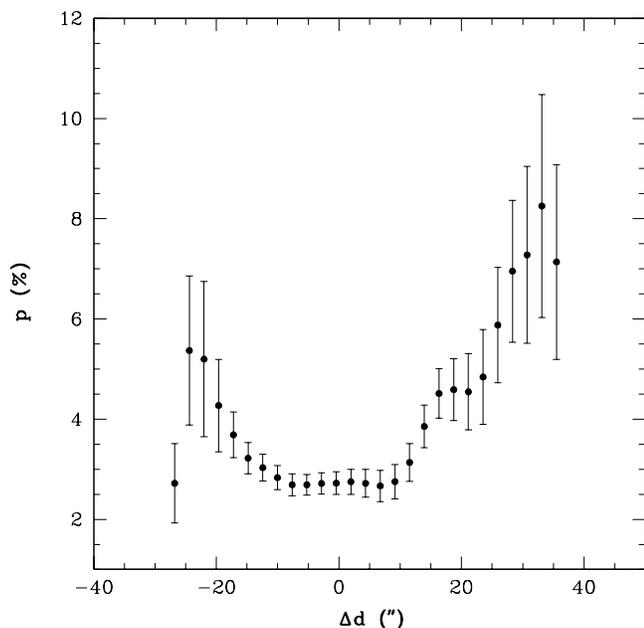
FIG. 2.—Variation in p_{db} along a line perpendicular to the filament. These data are centered on $\alpha_{1950} = 5^h32^m52^s5$ and $\delta_{1950} = -5°02'46''$, the position of the source MMS 4 identified by Chini et al. (1997) and identified by the red cross in Fig. 1. The cut is centered on MMS 4, and Δd is the offset perpendicular to the filament. The plot clearly shows a reduction in polarization toward the center of the filament. The error bars represent the uncertainty associated with each interpolated data point. The depolarization effect cannot be accounted for merely by the increasing noise in regions of low signal. Only data points with $\sigma_p > 2.5$ were used.

peaked at $-33° \pm 5°$ and $-47° \pm 15°$. Since the maximum uncertainty associated with any value of θ is $12°$, region D is the only one where no alignment exists between the filament and the polarization pattern.

In short, the polarization, and hence inferred field direction (in the plane of the sky), $B_\perp$, changes as one moves along OMC-3. $B_\perp$ is predominantly perpendicular to the filament along most of its length, diverging by $30°-50°$ from the filament only in the southernmost part of OMC-3. These results are roughly consistent with the work of Schleuning (1998), which also established $B_\perp$ perpendicular to the filament direction in OMC-1. The field direction does not appear to be affected by the presence of the dust condensations, but rather is aligned with the structure of the filament itself. At a resolution of $15''$ (7500 AU), these data simply may not have enough resolution to detect the details of fields associated with the starless cores or protostellar envelopes and their associated outflows.

3.2. The Influence of Outflows?

Many previous works have noted that the inferred $B_\perp$ field direction from long-wavelength polarization is oriented either parallel (e.g., *IRAS* 16293, Tamura et al. 1993; NGC 1333, Minchin, Sandell, & Murray 1995; Tamura, Hough, & Hayashi 1995) or perpendicular (e.g., VLA 1623, Holland et al. 1996) to the observed protostellar outflow direction. The relative orientations of the outflows in OMC-3 are illustrated by the green lines on Figure 1, as measured by Chini et al. (1997) and Yu et al. (1997), using ^{12}CO $J = 2-1$ and H_2 shocks, respectively, to identify outflow signatures. With the exception of MMS 6, the outflows are aligned east-west. Hence, in regions A–C, the outflows are perpendicular neither to the filament nor the $B_\perp$-

field. In region D, they are aligned perpendicular to the filament, but are offset from $B_\perp$ by $\sim 30°-50°$; however, it is possible that we may be detecting a superposition of the magnetic fields of the filament and the outflow(s). Reipurth, Rodríguez, & Chini (1999) suggest that MMS 9 is, in fact, the driving source for the most powerful outflow in the OMC-3 region. If the evolutionary sequence proposed by Chini et al. (1997) is correct, then MMS 9's outflow may have had sufficient time to alter the magnetic field in its vicinity.

These results suggest that the field of the filament alone does not determine the outflow direction. Thus, there must be other relevant factors that determine the stucture of a protostellar system. Were these data interpreted as a uniform field along which material had collapsed, one would naively expect protostellar disks to be aligned parallel to the filament, and outflows perpendicular to it but aligned with the ambient field; however, this is not observed.

3.3. Percentage Polarization

The distribution of p_{db} along the filament exhibits a mean value of 4.2%, with a $1\ \sigma$ dispersion of 1%. Values up to 100% are allowed, but only those less than 20% (i.e., all but 27) are plotted on Figure 1 since larger values are unlikely to be physical. The rms dp and σ_p values of unplotted data are 15% and 2.9, compared to 2.5% and 7.3 for all values of p with $\sigma_p > 2.5$. Polarizations up to 11.9% have been detected with $\sigma_p \sim 7$.

Several authors have discussed whether observations of decreased polarization percentage toward regions of higher flux are due to changes in physical conditions or averaging of small scale variations in a large beam. Figure 2 shows the percentage polarization along a cut perpendicular to the filament centered on MMS 4 (indicated by the *red cross* in Fig. 1), which has the highest σ_p in our data set. Although the uncertainties are increasing toward the edge of the filament, the data show a clear trend of decreasing polarization percentage toward the filament's center. These changes could be due to changes in either grain properties or field strength, but they have also been suggested as an observable signature of helical fields (Fiege & Pudritz 2000). The interpretation of this depolarization effect will be discussed more fully in a forthcoming paper.

4. SUMMARY

Submillimeter wavelength polarimetry with the JCMT has revealed a highly ordered polarization pattern along the filament known as OMC-3. These data indicate that $B_\perp$ is perpendicular to the filament along most of its length, diverging only in the most southern regions by between $30°$ and $50°$. The outflows that have been observed in OMC-3 are aligned with neither the ambient field nor the filament in any consistent way. The field of the filament is thus unlikely to be the dominant factor in determining the configuration of the protostellar systems embedded within it. The mean percentage polarization is 4.2%, with a $1\ \sigma$ dispersion of 1%. Values as high as 11.9% have been measured with $\sigma_p \sim 7$. A depolarization effect is measured toward the denser parts of the filament.

REFERENCES

Bally, J., Langer, W. D., Stark, A. A., & Wilson, R. W. 1987, ApJ, 313, L45
Castets, A., & Langer, W. D. 1995, A&A, 294, 835
Chini, R., Reipurth, B., Ward-Thompson, D., Bally, J., Nyman, L.-Å., Sievers, A., & Billawala, Y. 1997, ApJ, 474, L135
Draine, B. T., & Weingartner, J. C. 1996, ApJ, 470, 551
———. 1997, ApJ, 480, 633
Fiege, J., & Pudritz, R. 2000, MNRAS, 311, 85
Goodman, A. A., Jones, T. J., Lada, E. A., & Myers, P. C. 1995, ApJ, 448, 748
Heiles, C., Goodman, A. A., McKee, C. F., & Zweibel, E. G. 1993, in Protostars & Planets III, ed. E. H. Levy & J. I. Lunine (Tucson: Univ. Arizona Press), 279
Holland, W., Greaves, J., Ward-Thompson, D., & André, P. 1996, A&A, 309, 267
Johnstone, D., & Bally, J. 1999, ApJ, 510, L49
Kutner, M. L., Evans, N. J., II., & Tucker, K. D. 1976, ApJ, 209, 452
Lazarian, A., Goodman, A. A., & Myers, P. C. 1997, ApJ, 490, 273
Minchin, N., Sandell, G., & Murray, A. 1995, A&A, 293, L61
Myers, P. C., & Goodman, A. A. 1991, ApJ, 373, 509
Purcell, E. M. 1975 in Dusty Universe, ed. G. B. Field & A. G. W. Cameron (New York: Neal Watson), 155
———. 1979, ApJ, 231, 404
Reipurth, B., Rodríguez, L. F., & Chini, R. 1999, AJ, 118, 983
Schleuning, D. A. 1998, ApJ, 493, 811
Shu, F. H., Adams, F. C., & Lizano, S. 1987, ARA&A, 25, 23
Spitzer, L., Jr., & McGlynn, T. A. 1979, ApJ, 231, 417
Tamura, M., Hayashi, S., Yamashita, T., Duncan, W., & Hough, J. 1993, ApJ, 404, 21
Tamura, M., Hough, J., & Hayashi, S. 1995, ApJ, 448, 346
Yu, K. C., Bally, J., & Devine, D. 1997, ApJ, 485, L45